FULL PAPER

Solar Cells

**ADVANCED
ENERGY
MATERIALS**

www.advenergymat.de

Feasible D1–A–D2–A Random Copolymers for Simultaneous High-Performance Fullerene and Nonfullerene Solar Cells

Mingyu Jeong, Shanshan Chen, Sang Myeon Lee, Zhiwei Wang, Yankang Yang, Zhi-Guo Zhang, Chunfeng Zhang, Min Xiao, Yongfang Li, and Changduk Yang*

A series of PBDB-TTn random donor copolymers is synthesized, consisting of an electron-deficient benzo[1,2-c:4,5-c']dithiophene-4,8-dione (BDD) unit and different ratios of two electron-rich benzo[1,2-b:4,5-b']dithiophene (BDT) and thieno[3,2-b]thiophene (TT) units, with intention to modulate the intrachain and/or interchain interactions and ultimately bulk-heterojunction morphology evolution. A comparative study using 4×2 polymer solar cell (PSC) performance maps and each of the [6,6]-phenyl-C_{71}-butyric acid methyl ester ($PC_{71}BM$) and the fused-aromatic-ring-based molecule (m-ITIC) acceptors are carried out. Given the similarities in their absorption ranges and energy levels, the PBDB-TTn copolymers clearly reveal a change in the absorption coefficients upon optimization of the BDT to TT ratio in the backbone. Among the given acceptor combination sets, superior performances are observed in the case of PBDB-TT5 blended with $PC_{71}BM$ ($8.34 \pm 0.10\%$) or m-ITIC ($11.10 \pm 0.08\%$), and the dominant factors causing power conversion efficiency differences in them are found to be distinctly different. For example, the performances of $PC_{71}BM$-based PSCs are governed by size and population of face-on crystallites, while intermixed morphology without the formation of large phase-separated aggregates is the key factor for achieving high-performance m-ITIC-based PSCs. This study presents a new sketch of structure–morphology–performance relationships for fullerene- versus nonfullerene-based PSCs.

1. Introduction

At present, polymer solar cells (PSCs) based on conjugated polymers such as electron donors blended with fullerenes (e.g., [6,6]-phenyl-C_{71}-butyric acid methyl ester ($PC_{71}BM$)) as electron acceptors have been the leading candidates in

organic photovoltaic technology and have achieved power conversion efficiency (PCE) exceeding 10% by using a single bulk-heterojunction architecture.[1] Such great advances in PSCs based on fullerene acceptors are essentially fueled by their high electron mobility and isotropic electron transfer nature.[2] However, fullerenes are not ideal electron acceptors due to many intrinsic issues such as weak light absorption and unoptimized energy levels, which limit the design adaptability of the electron donor pair. Therefore, there is significant interest in developing alternative nonfullerene acceptors to resolve these drawbacks and to ultimately overcome the PCE bottleneck associated with fullerene-based PSCs.[3]

A breakthrough in nonfullerene acceptors occurred recently with the development of fused-aromatic-ring-based molecules such as ITIC and m-ITIC by Zhan and co-workers and Li and co-workers,[3d,4] demonstrating superior performance in blended films with polymer donors. Thereafter, a series of publications followed, shedding light on their many advantages over fullerenes such as synthetic flexibility, easy tunability of optical and electronic properties, and good stability of morphology.[5] However, in most cases, owing to the distinct conjugated skeletons of fullerene- and ITIC-based acceptors (nearly isotropic π-orbital versus highly anisotropic π-orbital), those state-of-art donor polymers in fullerene-based PSCs may not be the best

M. Jeong, S. Chen, S. M. Lee, Prof. C. Yang
Department of Energy Engineering
School of Energy and Chemical Engineering
Perovtronics Research Center
Low Dimensional Carbon Materials Center
Ulsan National Institute of Science and Technology (UNIST)
50 UNIST-gil, Ulju-gun, Ulsan 44919, South Korea
E-mail: yang@unist.ac.kr

Z. Wang, Prof. C. Zhang, Prof. M. Xiao
National Laboratory of Solid State Microstructures
School of Physics, and Collaborative Innovation Center of Advanced
Microstructures
Nanjing University
Nanjing 210093, China

Y. Yang, Prof. Z.-G. Zhang, Prof. Y. Li
Beijing National Laboratory for Molecular Sciences
CAS Key Laboratory of Organic Solids
Institute of Chemistry
Chinese Academy of Sciences
Beijing 100190, China

**ADVANCED
SCIENCE NEWS**
www.advancedsciencenews.com

**ADVANCED
ENERGY
MATERIALS**
www.advenergymat.de

matching donors in nonfullerene PSCs and vice versa.[6] Therefore, it is very challenging to develop high-performance polymer donors that are simultaneously compatible with $PC_{71}BM$- and ITIC-based acceptors in PSCs. Moreover, even subtle modifications to the chemical structures of the polymers can markedly alter their surface energies, segmental interactions, and segment rigidity, all of which can influence the morphology of the resultant active layer and the distribution of components within the active layer and at interfaces. Recently, random copolymerization has emerged as a promising synthetic strategy for fine-tuning the morphology (e.g., crystallinity and orientation), charge transport ability, electronic energy levels, and band gaps.[7] This can easily be correlated with photovoltaic parameters such as J_{SC}, V_{OC}, and FF to optimize the molecular structure to achieve high photovoltaic performance.

In this study, we utilized the random copolymerization approach with rigid, coplanar aromatic benzo[1,2-*b*:4,5-*b'*]dithiophene (BDT) and thieno[3,2-*b*]thiophene (TT) electron-rich units and benzo[1,2-*c*:4,5-*c'*]dithiophene-4,8-dione (BDD) electron-deficient unit to generate a series of PBDB-TT*n* random copolymers with *n*% of TT ratio, based on famous donor polymer PBDB-T. The fused TT unit has a strong tendency to form a large orbital overlapping area, which is highly beneficial for charge carrier transport through intermolecular hopping.[8] Therefore, we anticipated that incorporating the optimal fused TT content into the polymer backbone can help to circumvent the disadvantages on molecular packing and charge transport characteristics caused by the irregular sequence in the random copolymer strategy. In addition to a systematic study of their optical, electronic, and electrical properties, we applied four PBDB-TT*n* in both $PC_{71}BM$- and *m*-ITIC-based PSCs to build up the comparative 4 × 2 PSC maps and to identify the origins and key factors of the differences in direct performance comparisons. Among the copolymers, PBDB-TT5 demonstrated the best performances simultaneously in both given sets based on $PC_{71}BM$ (PCE = 8.34 ± 0.10%) and *m*-ITIC (PCE = 11.10 ± 0.08%) acceptors. From the detailed studies, we established a structure–morphology–performance relationship, thus providing a reliable method for developing compatible polymers for both high-performance fullerene and nonfullerene PSCs.

2. Results and Discussion

2.1. Synthesis and Characterization of Copolymers

The synthetic routes and chemical structures of the PBDB-TT*n* copolymers are shown in **Scheme 1**. Different feed ratios of donor monomers (BDT to TT = 100:0, 95:5, 90:10, and 80:20) were used during palladium-catalyzed Stille polymerization to produce PBDB-TT0,[9] PBDB-TT5, PBDB-TT10, and PBDB-TT20, respectively, where the number (*n*) indicates the donor content of TT in percent. Details of synthesis and characterization are given in the Experimental Section. Note that PBDB-TT20 showed somewhat limited solubility due to its higher content of the rigid fused-ring TT unit without any side chain in the main backbone, and thus total TT content of up to 20% was selected in this study.

To rule out aggregation-induced overestimation of molecular weight at room temperature, average molecular weights (M_{nS})
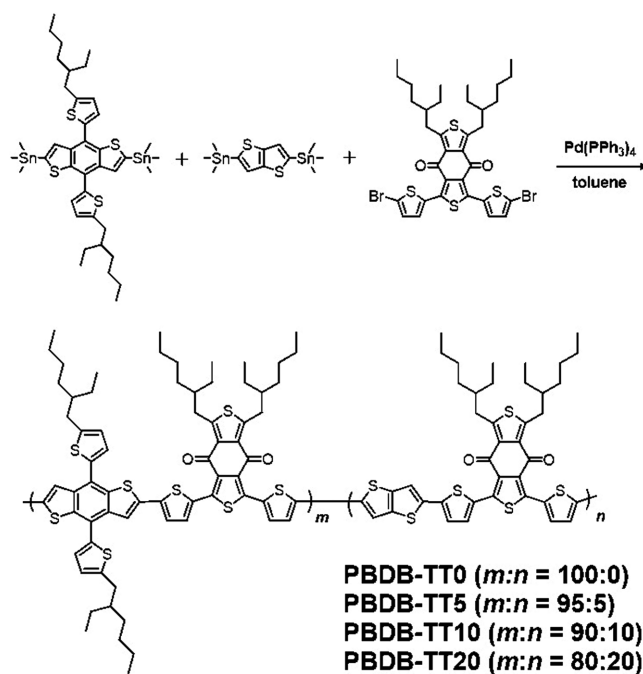
Scheme 1. Synthetic routes of the four PBDB-TT*n* copolymers via Stille polymerization.

were determined using high-temperature gel-permeation chromatography (HT-GPC) at 120 °C with 1,2,4-trichlorobenzene as the eluent, and the relevant data are summarized in **Table 1**. The four copolymers had M_n values of 11.7–24.8 kDa with polydispersities (PDI) of 2.50–4.12. The observed relatively lower M_n and the larger PDI of PBDB-TT20 compared to the other three copolymers might be caused by its decreased solubility. The chemical structures and high purity of the copolymers are verified by ^{1}H NMR spectroscopy, but determining the composition of BDT to TT through the integral ratios of the proton signals is rather difficult because of their broadening and overlapping in the aromatic region (see Figures S3–S5, Supporting Information). Thereby, we attempted to acquire high-temperature 2D NMR spectra, such as homonuclear correlation spectroscopy (COSY) and heteronuclear single quantum correlation (HSQC), where two samples (PBDB-TT0 and PBDB-TT20) were selected for 2D NMR because of their distinct difference in TT content in the random backbones. As seen in **Figure 1**b,e, ^{1}H-^{1}H COSY spectra of both polymers display three diagonal correlation peaks (A at 7.81 ppm (H_a), B at 7.39 ppm (H_b, H_d), and C at 7.1 ppm (H_c, H_e)) with two off-diagonal correlation peaks due to ethylhexyl-thienyl protons (H_b, H_c) of BDT moiety and thiophene spacer protons (H_d, H_e) of BDD moiety. On the other hand, two weak carbon-proton correlation peaks are visible in ^{13}C-^{1}H HSQC spectra of both samples (Figure 1c,f); one carbon peak at 128.4 ppm is correlated with the coupling of H_b, H_d while, the other carbon peak at 125.8 ppm is ascribed to the coupling of H_c, H_e.

Nevertheless, we realized that 2D NMR techniques could not unambiguously provide useful information about the composition because of the absence of H_f corresponding to TT protons. Instead, the actual ratios of BDT and TT in each copolymer were verified by carbon, hydrogen, and sulfur (CHS) elemental

**ADVANCED
SCIENCE NEWS**
www.advancedsciencenews.com

**ADVANCED
ENERGY
MATERIALS**
www.advenergymat.de

Table 1. Optical and electrochemical properties, molecular weight, and PDI values of PBDB-TT*n* copolymers.

	λ_{max}^{sol} [nm]	λ_{max}^{film} [nm]	λ_{onset} [nm]	E_g^{opt} [eV]	E_{HOMO}	E_{LUMO}	E_g^{CV}	M_n [kDa]	PDI
PBDB-TT0	617	621	697	1.78	−5.47	−3.54	1.93	15.3	3.21
PBDB-TT5	616	623	699	1.77	−5.45	−3.54	1.91	24.8	2.50
PBDB-TT10	580	584	698	1.78	−5.44	−3.54	1.90	18.6	3.50
PBDB-TT20	581	586	699	1.77	−5.43	−3.56	1.87	11.7	4.12

analysis (EA), where the EA data of the copolymers are within 0.31% of their theoretical values.

The optical properties of all copolymers were investigated by UV–visible absorption spectroscopy in chlorobenzene solution and thin films. No obvious red-shifted transition observed in the absorption spectroscopy from solution to film states. It can be attributed to the aggregation of BDD-based copolymers in the solution even at room temperature (**Figure 2**). Raising the temperature induces a continuous degradation of the low-energy absorption features of the copolymers in the solution (Figure S2, Supporting Information), that is, the intensity of the 0–0 vibrational transition relative to that of the 0–1 vibrational transition is decreased, which directly supports their aggregation properties in the solution state.[9,10] Specifically, the 0–1 peak intensity of PBDB-TT5 is somewhat insensitive

even at the evaluated temperatures compared to that of other samples, suggesting its stronger formation of aggregates in the solution. In addition, a closer look reveals less-resolved vibronic features in both the solution and the film states with higher TT content in the backbone, which suggests that further increasing the TT contents fraction over 10% in the polymer backbone would reduce the aggregation of PBDB-TT*n* copolymers.

Moreover, it is also interesting to note that the film absorption coefficients exhibit the following order: PBDB-TT0 < PBDB-TT20 < PBDB-TT10 < PBDB-TT5 (Figure S1, Supporting Information). This observation is in contrast to the general conception used in many conjugated polymer systems, in which alternating copolymers have higher coefficients compared to random copolymers owing to stronger interchain interactions
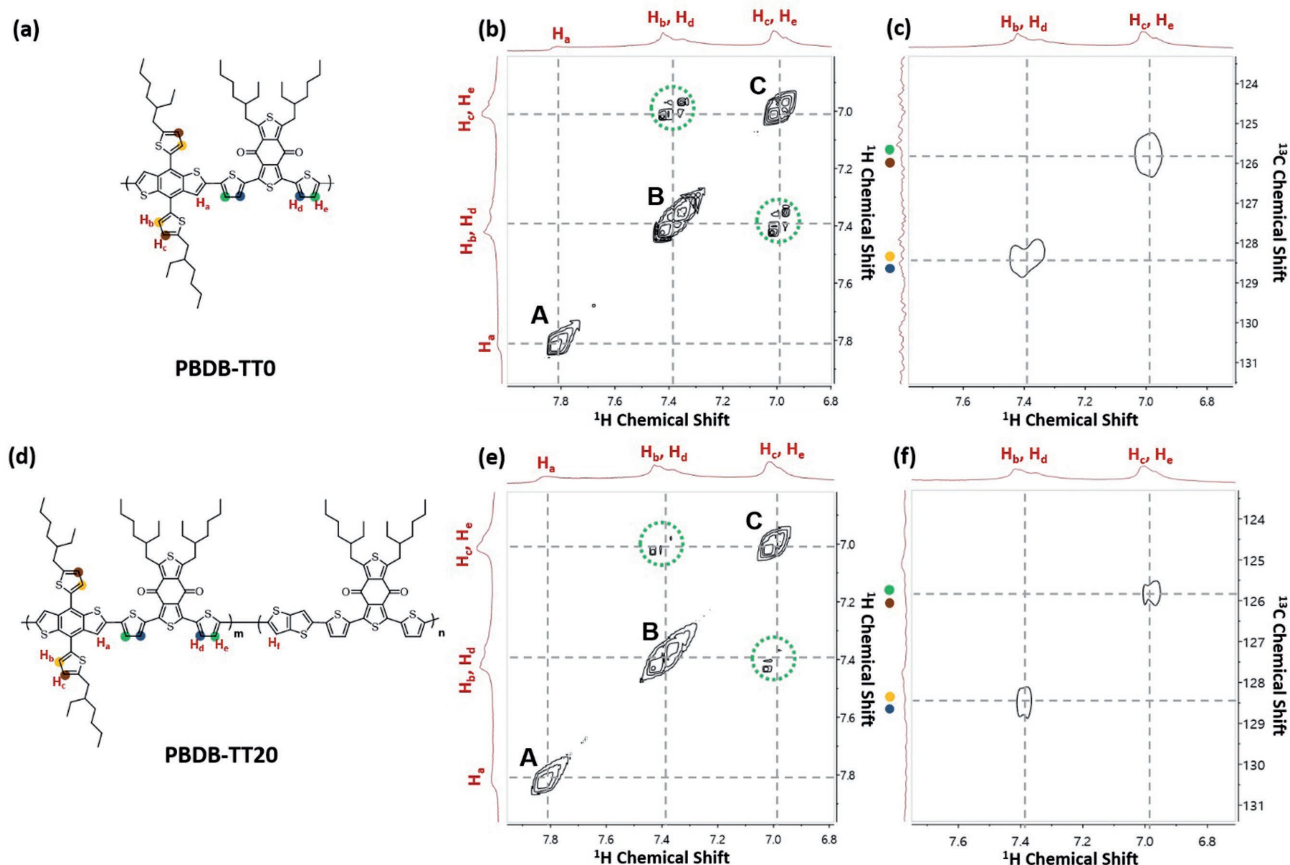

Figure 1. Chemical structures of a) PBDB-TT0 and d) PBDB-TT20 for 2D NMR measurement. b) 2D ¹H–¹H correlation COSY spectrum and c) 2D ¹³C–¹H correlation HSQC spectrum of PBDB-TT0. e) 2D ¹H–¹H correlation COSY spectrum and f) 2D ¹³C–¹H correlation HSQC spectrum of PBDB-TT20. All measurements were acquired at 80 °C with 1,1,2,2-tetrachloroethane as a solvent.
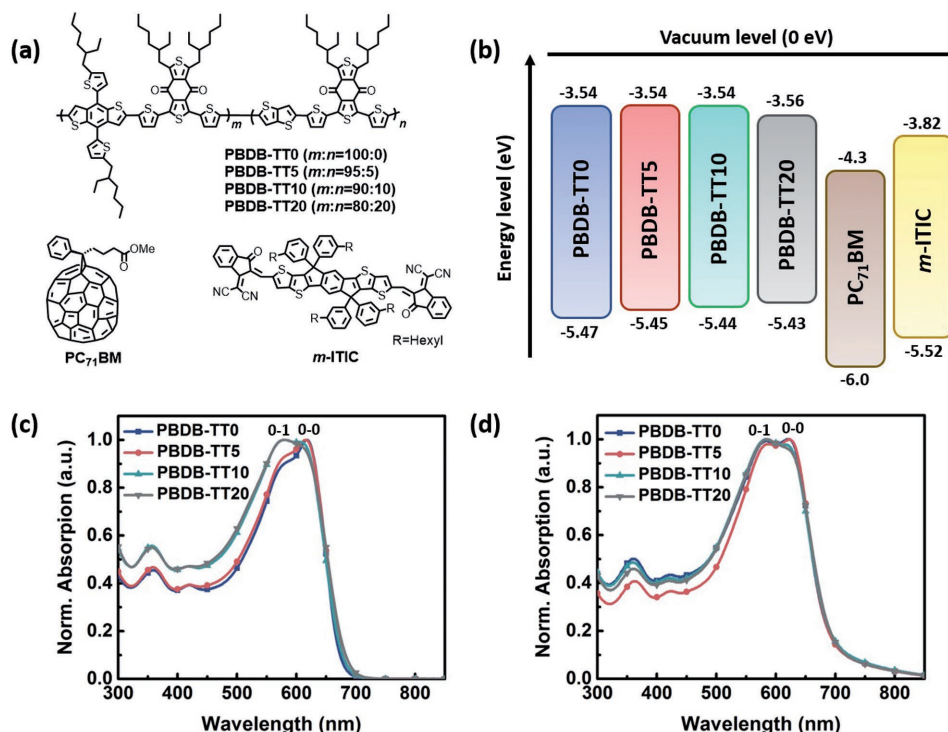
**ADVANCED
SCIENCE NEWS**

www.advancedsciencenews.com

**ADVANCED
ENERGY
MATERIALS**

www.advenergymat.de

Figure 2. PBDB-TT*n* copolymers and corresponding optical and electrochemical properties. a) Chemical structures of four PBDB-TT*n* copolymers, PC$_{71}$BM, and *m*-ITIC. b) Energy level diagrams of four PBDB-TT*n* copolymers, PC$_{71}$BM, and *m*-ITIC. c) UV–Vis spectra of PBDB-TT*n* copolymers in chlorobenzene solution. d) UV–Vis absorption spectra of four neat polymers as thin film.

induced by the regular monomer sequence.[11] We speculate the introduction of planar-fused TT units into the backbones potentially offers a beneficial trade-off that allows for effective molecular packing of the random copolymers even with non-periodic sequence distribution. The optical band gaps E_g^{opt} estimated from the film absorption edges of the copolymer series are nearly identical (1.77–1.78 eV).

Cyclic voltammetry was used to determine the highest-occupied molecular orbital (E_{HOMO}) and lowest-unoccupied molecular orbital (E_{LUMO}) levels of the copolymers (Figure S6, Supporting Information). As summarized in Figure 2b, all copolymers have very similar E_{HOMO} ($\approx$–5.45 eV) and E_{LUMO} ($\approx$–3.55 eV) levels, suggesting that introduction of the TT units did not significantly influence their frontier energy orbitals. Note that the LUMO offsets between the donor copolymers and the two acceptors (PC$_{71}$BM and *m*-ITIC) are higher than 0.26 eV, thus providing an affordable driving force for efficient photoinduced electron transfer, whereas the HOMO offset between the donor copolymers and *m*-ITIC is very small. The efficient acceptor-to-donor hole transfer still occurred in the PBDB-TT*n*:*m*-ITIC blends, as testified by transient absorption (TA) measurement in the following photophysics section, indicating a relatively low photon energy loss in this combination system.

2.2. Photovoltaic Properties

The photovoltaic properties of the PBDB-TT*n* copolymer systems blended with either PC$_{71}$BM or *m*-ITIC were evaluated using a

conventional single-cell device with the configuration of ITO (indium-tin oxide)/poly(3,4-ethylenedioxythiophene):poly(styrenesulfonate) (PEDOT:PSS)/active layer/perylenediimide functionalized with amino *N*-oxide (PDINO)[12]/Al. Optimal active layers with a thickness of $\approx$90 ± 10 nm were fabricated by spin-coating using either the PBDB-TT*n*:PC$_{71}$BM (1:1 wt%) *ortho*-dichlorobenzene (*o*-DCB) solution with 3 vol% 1,8-diiodooctane (DIO) or the PBDB-TT*n*:*m*-ITIC (1:1 wt%) chlorobenzene (CB) solution with 0.5 vol% DIO followed by thermal annealing at 150 °C for 10 min.

The current density–voltage (*J*–*V*) curves of the PSCs are plotted in **Figure 3**a, and the relevant photovoltaic parameters are summarized in **Table 2**. For the sake of clarifying the PBDB-TT*n*:acceptor blend systems in the following figures, we have abbreviated them as 0/PC$_{71}$BM, 5/PC$_{71}$BM, 10/PC$_{71}$BM, and 20/PC$_{71}$BM; and 0/*m*-ITIC, 5/*m*-ITIC, 10/*m*-ITIC, and 20/*m*-ITIC for the PBDB-TT*n*:PC$_{71}$BM and the PBDB-TT*n*:*m*-ITIC cases, respectively. First, the 0/PC$_{71}$BM control device showed a J_{SC} of 11.75 mA cm^{-2}, FF of 69.93%, and V_{OC} of 0.886 V, yielding a PCE of 7.28%, which is comparable to the value reported by Hou and co-workers.[9] Upon increasing the TT content in the donor polymer backbone, especially in the 5/PC$_{71}$BM device, the best PCE of 8.24% is obtained along with both a higher J_{SC} of 14.04 mA cm^{-2} and FF of 70.37%, but marginally depressed V_{OC} of 0.853 V. It can be seen for the given PC$_{71}$BM acceptor sets that the random copolymer-based PSCs significantly enhance the J_{SC} values, while the V_{OC}s values decrease with increasing TT content.

Interestingly, as for the PBDB-TT*n*:PC$_{71}$BM systems, in the given *m*-ITIC acceptor series, the random copolymer-based
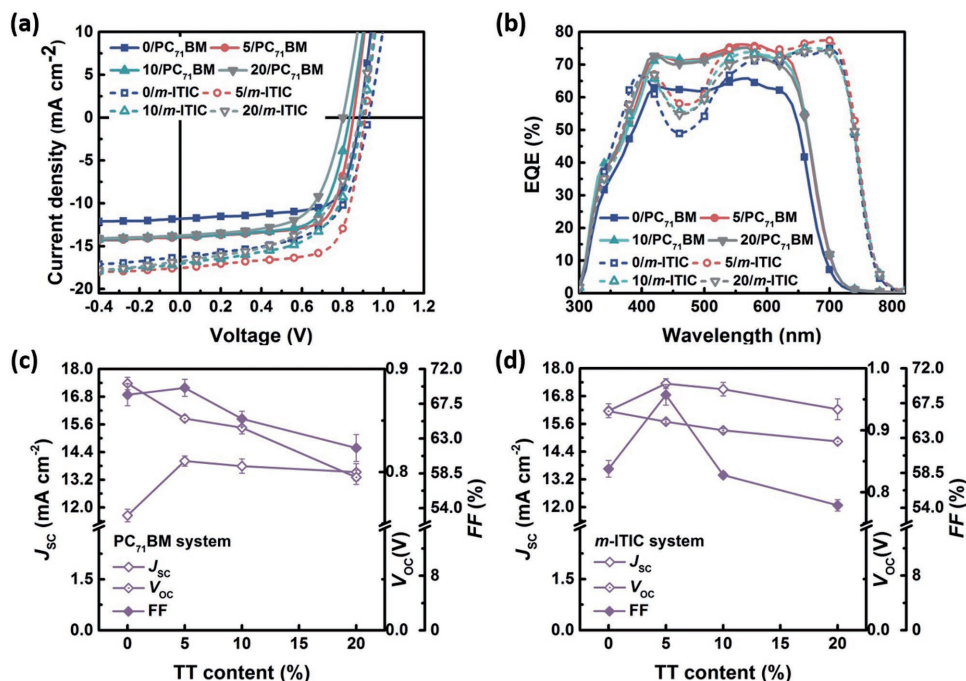
Figure 3. a) J–V curves of the PSCs based on PBDB-TTn:PC$_{71}$BM and PBDB-TTn:m-ITIC blend under 100 mW cm^{-2} AM 1.5G solar illumination. b) Corresponding EQE spectra. c) J_{SC}, V_{OC}, and FF values of the optimized PBDB-TTn:PC$_{71}$BM and d) PBDB-TTn:m-ITIC solar cells versus the TT content in the donor polymer.

PSCs showed higher J_{SC}s, but lower V_{OC}s compared to the control 0/m-ITIC device (J_{SC} = 16.27 mA cm^{-2}, V_{OC} = 0.93 V, FF = 60.04%, and PCE = 9.08%). Again, the best performance (PCE up to 11.17% with an enhanced J_{SC} of 17.53 mA cm^{-2}) was obtained for the PBDB-TT5:m-ITIC combination.

With comparative results for the PSCs employing PC$_{71}$BM and m-ITIC acceptors in hand (see the dependence of FF, J_{SC}, and V_{OC} values on the TT contents in Figure 3c,d), we find that the m-ITIC-based PSC combinations show somewhat lower FFs but much higher J_{SC} and V_{OC} values,

Table 2. Photovoltaic parameters of the solar cells based on PBDB-TTn:PC$_{71}$BM and PBDB-TTn:m-ITIC blend under the illumination of AM 1.5G, 100 mW cm^{-2}.

Blending system		V_{OC} [V]	J_{SC} [mA cm^{-2}]	FF [%]	PCE [%]	Calculated J_{SC} [mA cm^{-2}]
Acceptor	Donor					
PC$_{71}$BM	PBDB-TT0	0.886	11.75	69.93	7.28	11.29
		0.886 ± 0.006	11.65 ± 0.27	68.67 ± 1.42	7.16 ± 0.11	
	PBDB-TT5	0.853	14.04	70.37	8.42	13.37
		0.852 ± 0.003	14.01 ± 0.22	69.56 ± 1.10	8.34 ± 0.10	
	PBDB-TT10	0.836	13.90	66.79	7.76	13.21
		0.843 ± 0.006	13.79 ± 0.31	65.56 ± 0.99	7.59 ± 0.21	
	PBDB-TT20	0.803	13.78	62.04	6.86	13.09
		0.795 ± 0.007	13.53 ± 0.37	61.79 ± 1.74	6.67 ± 0.18	
m-ITIC	PBDB-TT0	0.930	16.27	60.04	9.08	15.45
		0.931 ± 0.006	16.17 ± 0.30	59.02 ± 1.07	8.98 ± 0.09	
	PBDB-TT5	0.913	17.53	69.79	11.17	16.69
		0.914 ± 0.003	17.34 ± 0.21	68.58 ± 1.33	11.10 ± 0.08	
	PBDB-TT10	0.900	17.06	58.54	8.99	16.21
		0.900 ± 0.003	17.10 ± 0.29	58.22 ± 0.40	8.87 ± 0.12	
	PBDB-TT20	0.885	16.81	54.38	8.09	15.98
		0.882 ± 0.005	16.23 ± 0.45	54.31 ± 0.73	7.90 ± 0.17	

**ADVANCED
SCIENCE NEWS**

www.advancedsciencenews.com

**ADVANCED
ENERGY
MATERIALS**

www.advenergymat.de

ultimately leading to better PCE compared to the corresponding $PC_{71}BM$-based ones. However, in both cases, the same trend for each photovoltaic parameter is observed as a function of the TT content in the main backbones. Therefore, we can reasonably infer that benefiting from both complementary absorption spectra and higher-lying LUMO levels of m-ITIC acceptor relative to $PC_{71}BM$ plays a dominant role in obtaining superior J_{SC} and V_{OC} values when using the m-ITIC-based PSC systems.[4b,5d,h]

External quantum efficiency (EQE) curves of all devices as a function of the wavelength of incident light are shown in Figure 3b. Clearly, the m-ITIC-based devices have much broader photoresponses, covering spectral regions of up to 800 nm, compared to the $PC_{71}BM$ acceptor-based devices, which are responsible for the significantly improved J_{SC} values in m-ITIC-based devices. Specially, the PBDB-TT5:m-ITIC blend has the highest photoresponse efficiency, with its maximum EQE value approaching 75% in the 700–800 nm spectral range. One can conclude that in addition to the enhanced photogenerated current density induced by broader and stronger absorptivity of m-ITIC relative to $PC_{71}BM$, controlling the TT content in the PBDB-TTn copolymers can effectively further increase their light-harvesting ability, which is a key matter for achieving high-performance PSCs.

2.3. Film Morphology

Since the inner physical mechanisms are strongly correlated to the morphological features of blend films, grazing incidence wide-angle X-ray scattering (GIWAXS) measurements were performed to define the morphology and molecular ordering of the neat copolymer films as well as of the blends.[13] As shown in **Figure 4**a and Figure S7 (Supporting Information), the four PBDB-TTn neat films show similar GIWAXS patterns with the lamellar (100) packing for both the out-of-plane (along q_z) and the in-plane (along q_{xy}) directions and strong π–π stacking (010) peaks along q_z, implying preferential formation of the face-on ordering. In addition, we determined the d-spacing distances and the coherence lengths ($CCL_{(010)}$) by using the out-of-plane (010) peaks (Figure 4b).

Even though nonlinear trends in both the d-spacing and CCL values are observed, PBDB-TT5 has a larger CCL with smaller d-spacing compared to the other samples, suggesting its relatively enhanced crystallinity with tighter π–π stacking.[5c–e,7d,14] This demonstrates that the incorporation of the optimal TT content in the random copolymer can induce more ordered structure and higher crystallinity of the polymer main chains.

Moreover, we constructed an intensity azimuthal pole figure for the (100) scattering peak, as shown in Figure 4c.
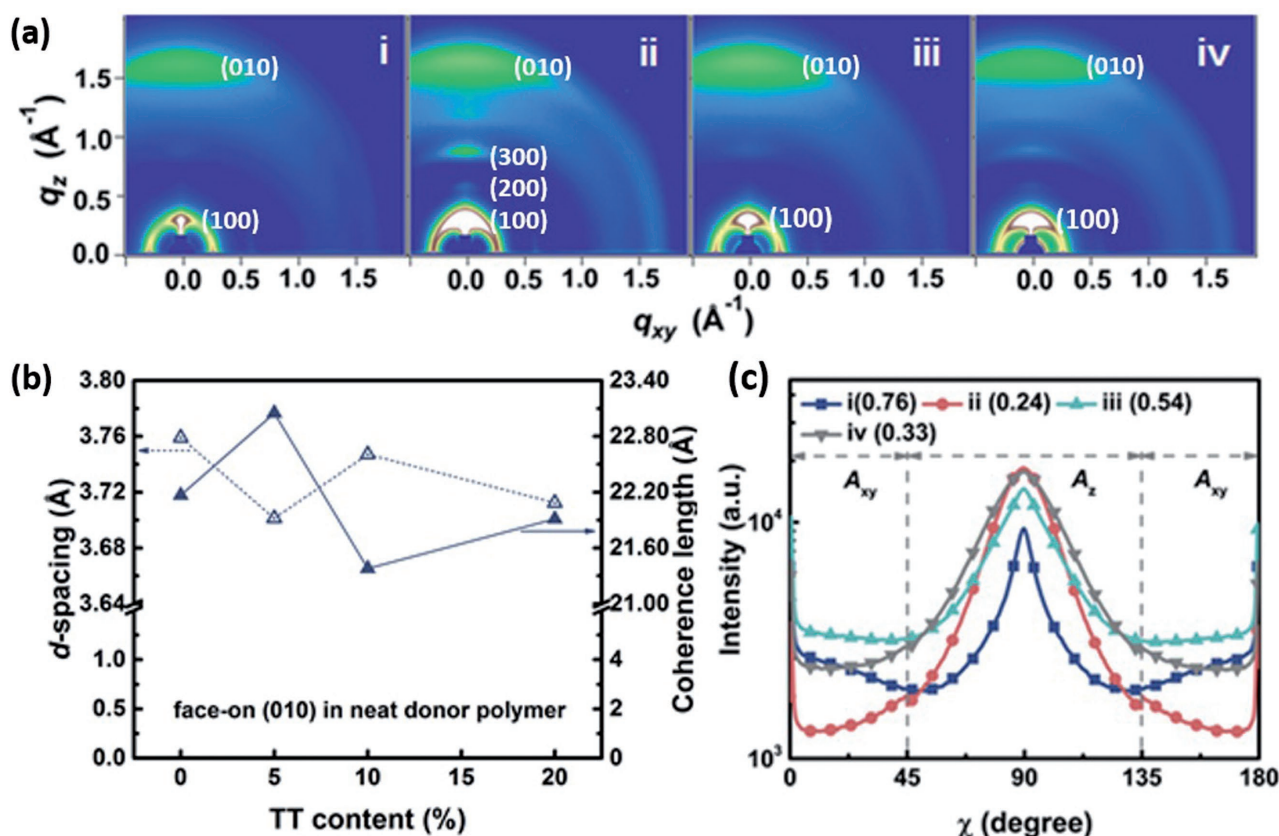

Figure 4. a) GIWAXS images of the neat PBDB-TTn donor polymer films: (i) PBDB-TT0, (ii) PBDB-TT5, (iii) PBDB-TT10, (iv) PBDB-TT20. b) The d-spacings and coherence lengths estimated from the face-on (010) diffraction in films versus the TT content in the donor polymer. c) The corresponding pole figure plots from the (100) lamellar diffraction in the PBDB-TTn films, the fraction values in parentheses are the ratios of integrated 0°–45° and 135°–180° (A_{xy}) to 45°–135° (A_z) area.

**ADVANCED
SCIENCE NEWS**
www.advancedsciencenews.com

**ADVANCED
ENERGY
MATERIALS**
www.advenergymat.de

The integrated areas within the azimuthal angle (χ) ranges of 0°–45° and 135°–180° (A_{xy}) and 45–135° (A_z) are defined as the corresponding fractions of face-on and edge-on crystallites, respectively, and the ratio of A_{xy}/A_z was calculated as a figure for the face-on to edge-on ratio. The alternating reference PBDB-TT0 copolymer has a higher A_{xy}/A_z value than those of the random copolymers, suggesting the existence of a larger population of face-on crystallites, which is probably due to the different preaggregation in the solvent and/or morphological evolution during film drying.

The GIWAXS patterns of PBDB-TTn copolymers blended with PC$_{71}$BM or m-ITIC are shown in **Figure 5**a and Figure S7 (Supporting Information). Note that the (010) π–π stacking peak intensities of the m-ITIC-based blends are relatively strong compared to those of the PC$_{71}$BM-based blends, which are likely due to the overlap of the π–π peaks induced by PBDB-TTn and m-ITIC. Thereby, appropriate correction and peak deconvolution were applied to obtain the individual (010) peak profiles for the blend cases (see Figure S8 in the Supporting Information for the detailed deconvolution procedure), and the calculated CCL$_{(010)}$ values were plotted against TT contents of the PBDB-TTn copolymers (Figure 5b,c). The PC$_{71}$BM blend systems maintain similar CCL$_{(010)}$ values for the PBDB-TTn copolymers ($\approx$31.50 Å) and the PC$_{71}$BM ($\approx$27.60 Å), respectively, whereas both components values of the m-ITIC blends vary substantially across TT contents, and the minimal values were achieved in the case of the PBDB-TT5:m-ITIC blend.

Moreover, the majority of face-on crystallite population is also identified by using $A_{xy}/(A_{xy} + A_z)$ for the (100) scattering peak in the blend systems (Figure 5c; Figure S10, Supporting Information). The following observations can be made:
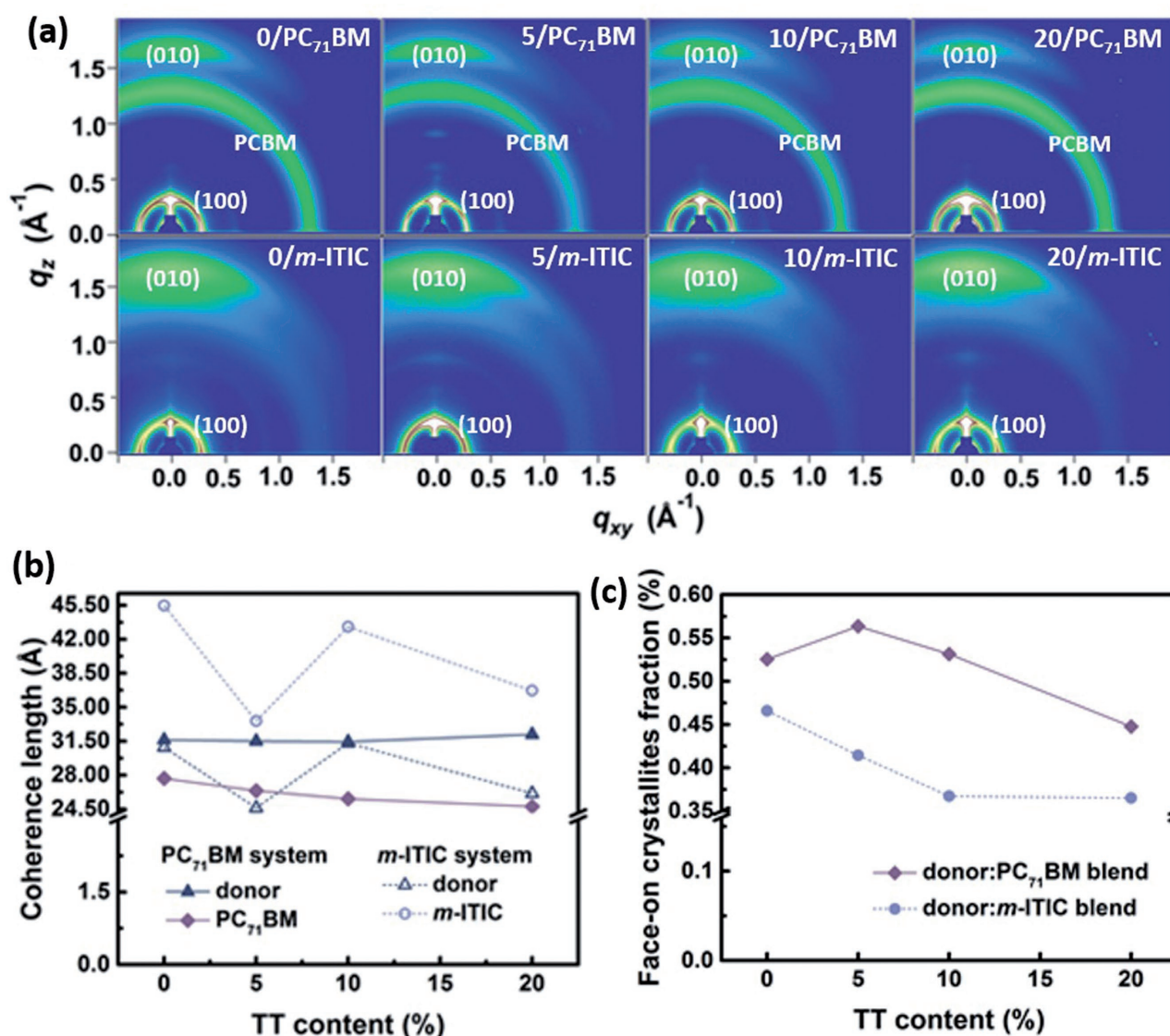

Figure 5. a) GIWAXS images of the PBDB-TTn:PC$_{71}$BM and PBDB-TTn:m-ITIC blend films. b) The coherence lengths estimated from the face-on (010) diffraction in the blend films versus the TT content in the donor polymer. c) The face-on crystallites fraction estimated from the (100) diffraction in the blend films versus the TT content in the donor polymers.

**ADVANCED
SCIENCE NEWS**

www.advancedsciencenews.com

**ADVANCED
ENERGY
MATERIALS**

www.advenergymat.de

(i) First, in the $PC_{71}BM$-based blend films, the calculated $A_{xy}/(A_{xy} + A_z)$ values are 0.526, 0.567, 0.531, and 0.446 for PBDB-TT0, PBDB-TT5, PBDB-TT10, and PBDB-TT20, respectively, suggesting that in the PBDB-TT5:$PC_{71}BM$ combination, there is a greater amount of crystalline domains with face-on orientations, which is beneficial for charge transport in the vertical channels across the electrodes.[15] It is noteworthy that the variation in the $A_{xy}/(A_{xy} + A_z)$ values shows the same trend as that in the J_{SC} and PCE values obtained for PBDB-TTn:$PC_{71}BM$ devices, implying that the difference in performance originates mainly from the different packing orientations in the blend films. (ii) Second, by contrast, the m-ITIC-based blend films show a generally decreased tendency toward face-on orientation with increasing TT contents. (iii) Third, regardless of the PBDB-TTn copolymers, the $PC_{71}BM$-based blend films have higher $A_{xy}/(A_{xy} + A_z)$ values than the m-ITIC-based blend films, indicating a more growing major population of face-on crystallites in the $PC_{71}BM$ blend films. Consequently, we are aware that the mechanism governing the photovoltaic process in m-ITIC-based PSCs is somewhat different from that in the conventional $PC_{71}BM$-based PSCs, in which high polymer crystallinity and face-on orientation are key factors for achieving high device performance.

To further establish the morphology–performance relationships of the $PC_{71}BM$ relative to that of the m-ITIC-based PSCs using the same copolymer platforms, the top surface and the bulk morphology of the blend films fabricated under the optimal conditions were investigated using atomic force spectroscopy (AFM) and transmission electron microscopy (TEM), respectively. Compared to the rough surfaces (root-mean-square (R_q) values: 1.95–3.12 nm) of the $PC_{71}BM$-based blends, relatively smooth surfaces with lower R_q values of 1.12–1.48 nm (see Figure S11, Supporting Information) were observed in the m-ITIC-based blends.

In addition, as shown in **Figure 6**, although some degree of phase separation could be found in the bulk features of both blend films, the donor–acceptor domains are only partially visible with granular-like aggregates in the TEM images of the m-ITIC-based blends, whereas the $PC_{71}BM$-based blends show well-defined fibril-like phase-separated microstructures. Especially, in case of the best-performing combination

(PBDB-TT5:m-ITIC), smaller aggregates were distributed more uniformly, implying suitable miscibility between the donor and the acceptor components. This is in good agreement with the $CCL_{(010)}$ results discussed above. The well-distributed microstructure with small-scale phase separation in PBDB-TT5:m-ITIC is expected to promote efficient exciton dissociation and charge transfer, which is certainly critical for the observed superior device performance.[16] Considering the above findings, one can speculate that the formation of finer phase-separation structures is a decisive factor in obtaining high J_{SC} and PCE values in m-ITIC-based PSCs.

2.4. Charge Generation, Dissociation, and Transport Properties

We then investigated the carrier hole (μ_h) and electron (μ_e) mobilities of all blends by using the space charge limited current (SCLC) method since they are important probes of charge transport in the direction perpendicular to the substrate. As shown in **Figure 7**a and Figure S13 (Supporting Information), the $PC_{71}BM$-based blends yield μ_h and μ_e mobilities in the ranges of 1.97×10^{-3}–2.56×10^{-3} cm^2 V^{-1} s^{-1} and 6.78×10^{-4}–1.26×10^{-3} cm^2 V^{-1} s^{-1}, respectively, which are nearly one order of magnitude higher than those obtained using the m-ITIC-based blends (μ_h: 1.16×10^{-3}–3.30×10^{-3} cm^2 V^{-1} s^{-1}, μ_e: 3.84×10^{-5}–1.30×10^{-4} cm^2 V^{-1} s^{-1}). The results can be understood from the viewpoint of the overall higher fraction of the face-on oriented crystallites in the $PC_{71}BM$-based blends, as shown by GIWAXS.

To gain deeper insight into the correlations, charge recombination in devices was evaluated by analyzing their J–V characteristics as a function of light intensity (P) (Figure 7b,c). In general, the J_{SC} and P values follow a power-law functional relationship, $J_{SC} \propto P^\alpha$, where α approaches unity when nongeminate recombination is negligible.[17] The $PC_{71}BM$-based devices exhibited higher α values (in the range of 0.969–0.997) than those of m-ITIC-based devices (α = 0.926–0.983), suggesting that nongeminate recombination is relatively suppressed in the $PC_{71}BM$-based devices. Note that for the PBDB-TT5 blends with either $PC_{71}BM$- or m-ITIC-, the lowest degree of nongeminate recombination is realized, as evidenced by the highest α values
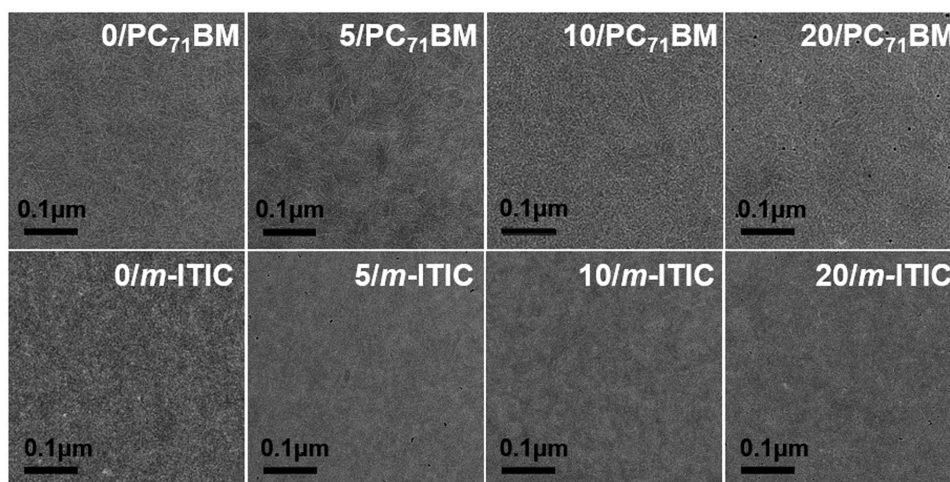

Figure 6. The TEM images of the PBDB-TTn:$PC_{71}BM$ and PBDB-TTn:m-ITIC blend films.
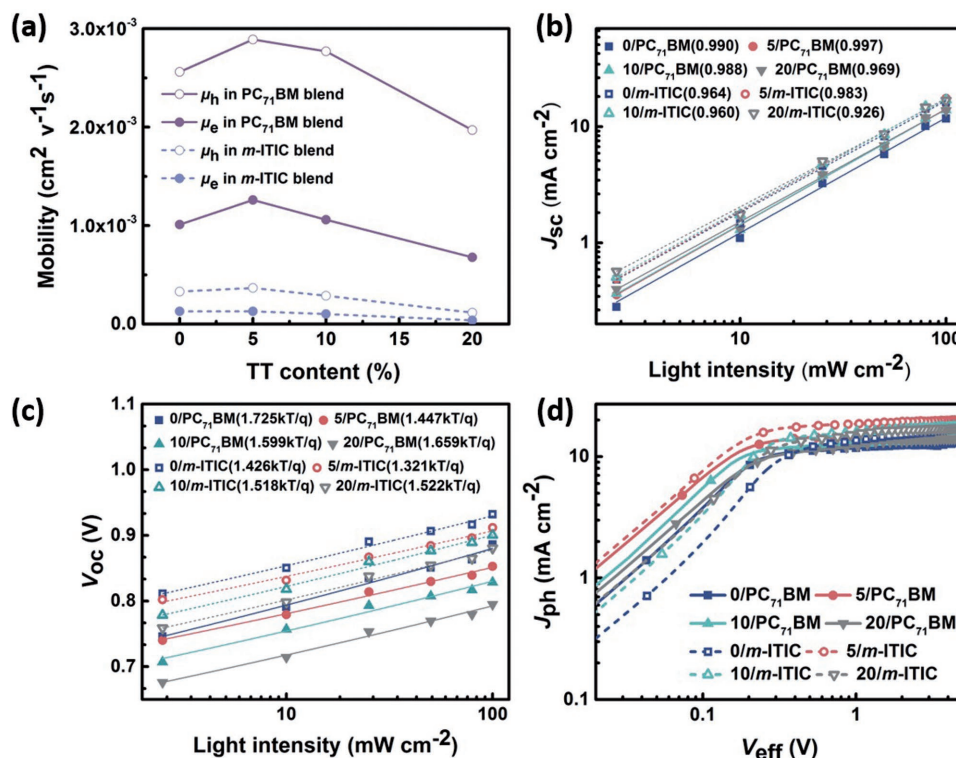
Figure 7. a) Hole and electron mobility of PBDB-TTn:PC$_{71}$BM and PBDB-TTn:m-ITIC blend. b) Light intensity dependence of J_{SC} and c) V_{OC} for the optimized devices. d) J_{ph} versus V_{eff} characterizes in the optimized devices.

of 0.997 and 0.983, respectively. The suppressed recombination mechanism correlates well with the observed higher charge mobilities, which is partially due to more efficient charge collection of the devices, thus accounting for the reduced build-up of space charges and resulting higher FF values of the PBDB-TT5-based devices compared with the other devices.[18]

The geminate or Shockley–Read–Hall recombination mechanism was extracted from the dependence of V_{OC} on P. The slope of V_{OC} versus the natural logarithm of P gives kT/q, where k, T, and q are the Boltzmann constant, temperature, and elementary charge, respectively.[17b,19] The magnitude of the slope represents the degree of geminate recombination during charge transport. The PC$_{71}$BM-based devices show slopes ranging from 1.447 to $1.725kT/q$, while the m-ITIC-based devices yielded slopes of $1.321–1.522kT/q$, indicating that geminate recombination occurs to a somewhat reduced extent in the m-ITIC sets.

Further studies on the exciton generation and dissociation rates were performed by plotting the photocurrent density (J_{ph}) versus effective voltage (V_{eff}) of the devices (Figure 7d). Here J_{ph} is defined as $J_{ph} = J_L − J_D$, where J_L and J_D are the photocurrent densities under illumination and in the dark, respectively; V_{eff} is given by $V_{eff} = V_0 − V_a$, where V_0 is the compensation voltage at $J_{ph} = 0$ and V_a is the applied voltage. Note that J_{ph} reaches the saturation value (J_{sat}) at $V_{eff} > 1.0$ V for all devices, at which point, all photogenerated excitons are dissociated into free charge carriers and collected at the electrodes. Among the blend samples, a higher J_{sat} value for PBDB-TT5:m-ITIC is observed, indicating a significant enhancement in exciton generation.

The exciton dissociation probabilities, P (E,T), defined as J_{ph}/J_{sat}, can be extracted from $J_{ph} − V_{eff}$ under the short-circuit condition. The calculated P (E,T) values in both the PC$_{71}$BM and the m-ITIC systems exhibit the following order: PBDB-TT20- < PBDB-TT0- < PBDB-TT10- < PBDB-TT5-based cells.

Moreover, it is clear that the P (E,T) values in the m-ITIC systems are higher than those of the corresponding PC$_{71}$BM ones. For example, PBDB-TT0:PC$_{71}$BM, PBDB-TT5:PC$_{71}$BM, PBDB-TT10:PC$_{71}$BM, and PBDB-TT20:PC$_{71}$BM have 87.17, 93.03, 91.41, and 82.99%, whereas PBDB-TT0:m-ITIC, PBDB-TT5:m-ITIC, PBDB-TT10:m-ITIC, and PBDB-TT20:m-ITIC possess 91.45, 93.28, 91.64, and 85.16%, respectivly. The results indicate that using m-ITIC within the sample donor platform reduces geminate recombination loss, originating from the previously described beneficial microstructural intermixing, facilitating exciton dissociation at the donor/acceptor interface. This might be the main reason for the superior J_{SC} values of m-ITIC devices, alongside their comprehensively enhanced light absorption properties. Collectively, the results obtained for different exciton dissociations and transport properties in the investigated devices were in close correlation with the morphology of the corresponding blends. Introducing an optimal ratio of TT units into the PBDB-TTn backbone leads to a better-performing donor–polymer match simultaneously for both the PC$_{71}$BM and the m-ITIC acceptors, although the operating mechanisms are different from each other. For example, in the case of the PC$_{71}$BM-based devices, high crystallinity and enhanced face-on crystallite fraction are responsible for higher J_{SC} and PCE. By contrast, in m-ITIC-based devices, in addition

**ADVANCED
SCIENCE NEWS**
www.advancedsciencenews.com

**ADVANCED
ENERGY
MATERIALS**
www.advenergymat.de

to complementary light absorption, the well-distributed nanostructural intermixing texture greatly suppresses charge recombination loss with improved exciton dissociation probability, which contributes toward the improved J_{SC}, FF, and PCE values.

2.5. Photophysics

To investigate different charge transfer kinetics between the fullerene and nonfullerene PSCs, TA measurements[5a,20] were carried out on high-performance blend films of PBDB-TT5:PC$_{71}$BM and PBDB-TT5:m-ITIC (**Figure 8**). Thanks to the well-separated absorption spectra of PBDB-TT5 and m-ITIC, the pump wavelengths of 500 and 730 nm were selected to excite PBDB-TT5 and m-ITIC, respectively. Using the pump wavelength of 730 nm (Figure S14, Supporting Information), only m-ITIC was excited as confirmed by the absence of the TA signal in the neat PBDB-TT5 film. Bleach signal at 736 nm which appeared in neat m-ITIC and blend films can be naturally ascribed to the ground state bleaching (GSB) of the transition in m-ITIC. Remarkably, clear bleach peaks at 588 and 640 nm gradually increase in TA spectrum of blend (Figure 8a). The spectral coverages are consistent with GSB features observed in neat PBDB-TT5 under ump at 500 nm. The build-up of these GSB signals is accompanied by a simultaneous decay of that in m-ITIC, suggesting the transfer of excitations from m-ITIC to PBDB-TT5. Since the excitation photon energy (at 730 nm) is much smaller than the absorption of PBDB-TT5, the bleach signal of polymer is unlikely to be contributed by the direct energy transfer process. It is safe to assign this excitation transfer to the process of hole transfer from m-ITIC to PBDB-TT5 which is also favored by the energy alignment of LUMO bands in the two materials. The rate of hole transfer is roughly estimated by the decay dynamics of GSB signals of m-ITIC in the neat and bland films (Figure S15, Supporting Information). The early-stage lifetime is shortened from ≈0.5 ps in the neat film to ≈0.17 ps in the blend film, implying highly efficient hole transfer in sub-ps temporal scale in nonfullerene PBDB-TT5:m-ITIC system. In the PC$_{71}$BM-based blend system, the spectral overlap of the absorption in PBDB-TT5 and PC$_{71}$BM makes it hard to selectively excite the donor or acceptor components. Figure 8d–f shows the TA dynamics of the blend sample under pump at 500 nm. The process of charge transfer is manifested as delay rises in the growth of PBDB-TT5 GSB signals (Figure 8e) and the photoinduced absorption in PC$_{71}$BM (Figure 8f). Because the processes of hole and electron transfer are entangled, it is difficult to accurately quantify the rate of hole transfer. Nevertheless, comparing with the GSB dynamics of PBDB-TT5 in the m-ITIC and PC$_{71}$BM-based blend systems, the buildup of GSB dynamics is found to be much faster in the PBDB-TT5:m-ITIC blend, implying a more efficient hole transfer in the PBDB-TT5:m-ITIC combination.

3. Conclusion

In summary, we synthesized and characterized a series of PBDB-TTn copolymers with BDD as an electron-deficient moiety and BDT together with TT as electron-rich units. Varying the BDT:TT compositions of the copolymers certainly affects their optical absorption coefficients due to the different degrees of intrachain and/or interchain interactions in thin films, rather than other properties such as absorption range, and frontier energy levels. We systematically investigated a
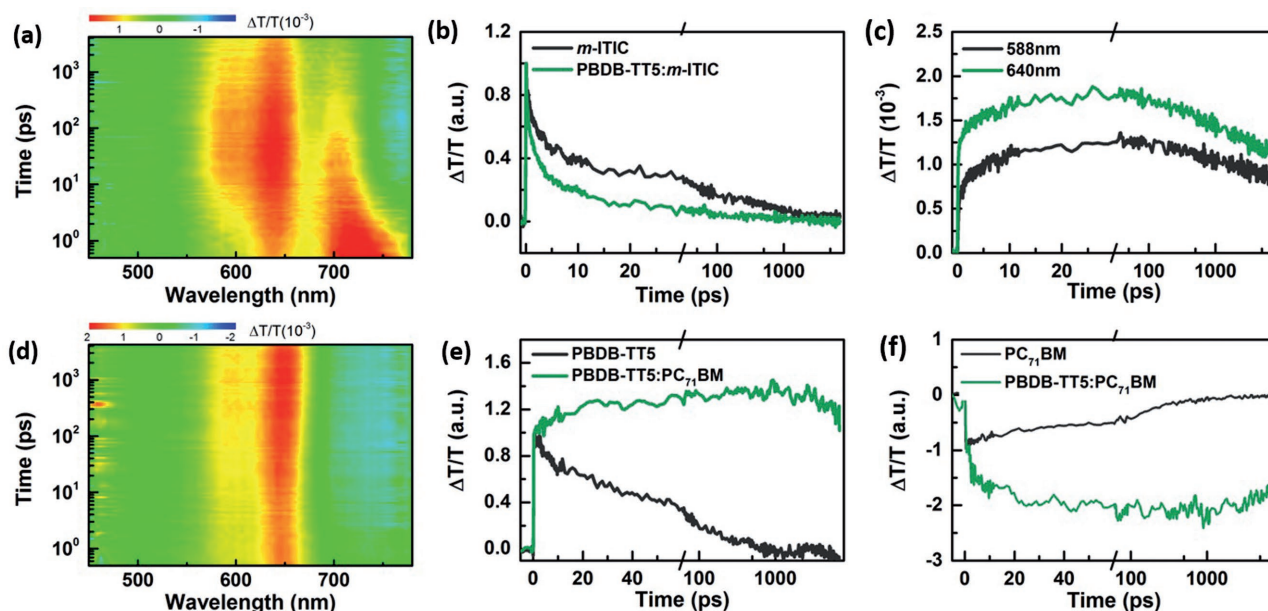

Figure 8. a–c) TA dynamics recorded from PBDB-TT5:m-ITIC blend with pump at 730 nm and d–f) PBDB-TT5:PC$_{71}$BM blend with pump at 500 nm, respectively. a) TA signal recorded from the film of PBDB-TT5:m-ITIC blend. b) Dynamics probed at 736 nm recorded from the neat m-ITIC and PBDB-TT5:m-ITIC blend films. c) Dynamic curves probed at 588 and 640 nm recorded from the PBDB-TT5:m-ITIC blend film. d) TA signal of PBDB-TT5:PC$_{71}$BM blend. e) Dynamics probed at 586 nm recorded from the neat PBDB-TT5, and PBDB-TT5:PC$_{71}$BM blend films. f) Dynamics probed at 730 nm recorded from the neat PC$_{71}$BM and PBDB-TT5:PC$_{71}$BM blend films.

**ADVANCED
SCIENCE NEWS**

www.advancedsciencenews.com

**ADVANCED
ENERGY
MATERIALS**

www.advenergymat.de

4 × 2 PSC matrix of PBDB-TTn-blend films employing either PC$_{71}$BM or m-ITIC acceptors. It was found that the m-ITIC-based devices showed better PCEs than the corresponding PC$_{71}$BM-based devices, which can be attributed to the enhanced photogenerated current density due to the broader and stronger absorptivity of m-ITIC relative to PC$_{71}$BM. Note that the PBDB-TT5 copolymer is the best-performing donor for each PC$_{71}$BM (PCE of 8.34 ± 0.10%) and the m-ITIC acceptor (PCE of 11.10 ± 0.08%). Based on the detailed morphology and electrical characteristics, we discovered that the photovoltaic performance of the PC$_{71}$BM-based devices is determined mainly the by degree of size and population of face-on crystallites, whereas in case of the m-ITIC-based devices, well-intermixed blend morphology is the dominant contributor. Not only does this study advance our understanding of the underlying operating mechanism of fullerene versus nonfullerene based on PSCs but it also demonstrates the high potential of simple random copolymerization for maximizing the performance of both types of PSCs.

4. Experimental Section

Materials and Measurements: 4,8-bis[5-(2-ethylhexyl)thiophen-2-yl]-2,6-bis(trimethylstannyl)benzo[1,2-b:4,5-b']dithiophene (BDT), 2,5-bis(trimethylstannyl)-thieno[3,2-b]thiophene (TT), and 1,3-dibromo-5,7-bis(2-ethylhexyl)benzo[1,2-c:4,5-c']-dithiophene-4,8-dione (BDD) were synthesized according to the previously reported methods.[9] ^{1}H NMR was recorded on a Varian VNRS 400 MHz (Varian, USA) spectrometer using CDCl$_3$ as solvent and tetramethylsilane as an internal reference. UV–Vis spectra were taken using a UV-1800 (SHIMADZU) spectrometer. Average number (M_n) and weight (M_w) molecular weights and PDI of the polymer products were determined by HT-GPC with Agilent 1200 HPLC and miniDAWN TREOS using a series of monodisperse polystyrene standards in 1,2,4-trichlorobenzene (HPLC grade) at 120 °C. CV measurement were performed on an AMETEK VersaSTAT 3 with a three-electrode cell in a nitrogen bubbled 0.1 M tetra-n-butylammonium hexafluorophosphate (n-Bu$_4$NPF$_6$) solution in acetonitrile at a scan rate of 0.1 V s^{-1} at room temperature. Ag/Ag+ (0.01 M of AgNO$_3$ in acetonitrile) electrode, platinum wire, and polymer coated glassy carbon electrode were used as the reference electrode, counter electrode, and working electrode, respectively. The Ag/Ag+ reference electrode was calibrated using a ferrocene/ferrocenium redox couple as an internal standard, whose oxidation potential is set at −4.8 eV with respect to zero vacuum level. The HOMO energy levels were obtained from the equation HOMO = −(E_{ox}^{onset} − $E_{(ferrocene)}^{onset}$ + 4.8) eV. The LUMO levels of polymers were obtained from the equation LUMO = −(E_{red}^{onset} − $E_{(ferrocene)}^{onset}$ + 4.8) eV. Elemental analysis was investigated using a Flash EA 2000 series at the Korea Basic Science Institute.

General Procedure for Random Polymers Using Stille Coupling: In a Schlenk flask, TT (a mol), BDT (b mol), and BDD ($a + b$ mol) were dissolved in anhydrous toluene (4 mL), and purged with argon for 15 min. Then, Pd(PPh$_3$)$_4$ (0.07 equiv. of BDD) was added and purged again with argon for 10 min. After that, the reaction mixture was stirred at 120 °C for 12 h. Afterward, small amounts of 2-bromothiophene and 2-(trimethylstannyl)thiophene were used as the end-capping agent, respectively. And then, the mixture was cooled down and precipitated to methanol. The precipitated crude product was purified via sequential Soxhlet extraction with methanol, acetone, hexane, and chloroform. The chloroform fraction was concentrated and precipitated to methanol. The purified copolymers were collected by using membrane filter (pore size, 0.45 µm) and dried under high vacuum oven.

PBDB-TT0: On basis of the procedure described above, the reference PBDB-TT0 copolymer was prepared by using BDT (100 mg, 0.111 mmol)

and BDD (84.8 mg, 0.111 mmol). Yield = 96.7%. M_n = 15.3 kDa, PDI = 3.21. Its NMR and EA data are well-consistent with the reported one.

PBDB-TT5: On basis of the procedure described above, BDT (95.4 mg, 0.105 mmol), TT (2.6 mg, 0.00555 mmol), and BDD (84.8 mg, 0.111 mmol) were used for copolymerization. Yield = 95.2%. M_n = 24.8 kDa, PDI = 2.50. ^{1}H NMR (400 MHz, CDCl$_3$), δ (ppm): 8.50 − 7.30 (br), 7.25 − 6.00 (br), 4.10 − 2.50 (br), 2.30 − 1.25 (br), 1.20 − 0.25 (br). Elemental analysis calculated for [C$_{666}$H$_{761}$O$_{20}$S$_{79}$]: C, 68.64; H, 6.74; S, 21.84; Found: C, 68.45; H, 6.72; S, 21.86.

PBDB-TT10: On basis of the procedure described above, BDT (90.3 mg, 0.0998 mmol), TT (5.2 mg, 0.0111 mmol), and BDD (84.8 mg, 0.111 mmol) were used for copolymerization. Yield = 94.9%. M_n = 18.6 kDa, PDI = 3.50. ^{1}H NMR (400 MHz, CDCl$_3$), δ (ppm): 8.50 − 7.30 (br), 7.25 − 6.00 (br), 4.10 − 2.50 (br), 2.30 − 1.25 (br), 1.20 − 0.25 (br). Elemental analysis calculated for [C$_{652}$H$_{742}$O$_{20}$S$_{78}$]: C, 68.41; H, 6.69; S, 22.04; Found: C, 68.43; H, 6.71; S, 22.11.

PBDB-TT20: On basis of the procedure described above, BDT (80.2 mg, 0.0887 mmol), TT (10.3 mg, 0.0222 mmol), and BDD (84.8 mg, 0.111 mmol) were used for copolymerization. Yield = 83.9%. M_n = 11.7 kDa, PDI = 4.12. ^{1}H NMR (400 MHz, CDCl$_3$), δ (ppm): 8.50 − 7.30 (br), 7.25 − 6.00 (br), 4.10 − 2.50 (br), 2.30 − 1.25 (br), 1.20 − 0.25 (br). Elemental analysis calculated for [C$_{624}$H$_{704}$O$_{20}$S$_{76}$]: C, 67.96; H, 6.57; S, 22.45; Found: C, 67.95; H, 6.58; S, 22.51.

Fabrication of Organic Solar Cell: The fullerene- and nonfullerene-based solar cells were fabricated with a configuration of ITO/ PEDOT:PSS/active layer/PDINO/Al. PEDOT:PSS (Bayer Baytron 4083) was spin-coated at 4000 rpm onto ITO substrate, followed by annealing at 140 °C for 20 min in air. The active layer was spin-coated from o-DCB/ DIO (v/v = 1/3 vol%) solutions with a donor/acceptor weight ratio of 1:1 wt% for PC$_{71}$BM systems, and CB/DIO (v/v = 1/0.5 vol%) solutions with a donor/acceptor weight ratio of 1:1 wt% for m-ITIC system, followed by thermal annealing at 150 °C for 10 min. Then methanol solution of PDINO (1.0 mg mL^{-1}) was then deposited atop the active layer with a spin rate of 3000 rpm for 60 s. Finally, 80 nm aluminum was thermally evaporated under vacuum (<5.0 × 10^{-5} Pa). The active area of each sample was 13.0 mm^2. The J–V characteristics were measured on Keithley 2400 source under illumination of an AM1.5G solar simulator with an intensity of 100 mW cm^{-2}. The EQE measurements were conducted in ambient air using an EQEs system (Model QEX7) by PV measurements Inc. (Boulder, Colorado). Hole and electron mobility were measured using the SCLC method. Device structures are ITO/ PEDOT:PSS/active layer/Au for hole-only devices and ITO/ZnO/active layer/PDINO/Al for electron-only devices. The SCLC mobilities were calculated by MOTT-Gurney equation

$$J = \frac{9\varepsilon_r\varepsilon_0\mu V^2}{8L^3} \tag{1}$$

where J is the current density, ε_r is the relative dieletiric constant of active layer material usually 2–4 for organic semiconductor, herein we use a relative dielectric constant of 4, ε_0 is the permittivity of empty space, μ is the mobility of hole or electron, and L is the thickness of the active layer, V is the internal voltage in the device, and $V = V_{Applied} − V_{Built-in} − V_{Series-resistane}$ (in the hole-only and the electron-only devices, the V_{bi} values are 0.2 and 0 V, respectively), where $V_{Applied}$ is the voltage applied to the device, and $V_{Built-in}$ is the built-in voltage resulting from the relative work function difference between the two electrodes. $V_{Series-resistane}$ is the voltage caused by the series and contact resistance potential drop ($V_{Series-resistane} = J \times R_{Series-resistane}$). For convenience, the voltage drop caused by this resistance ($R_{Series-resistane}$) was ignored.

Morphology Characterizations: An Agilent 5500 scanning probe microscope running with a Nanoscope V controller was used to obtain AFM images of polymer thin films. AFM images were recorded in high-resolution tapping mode under ambient conditions. Premium silicon cantilevers (TESP-V2) were used with a rotated tip to provide more symmetric representation of features over 200 nm. TEM

**ADVANCED
SCIENCE NEWS**

www.advancedsciencenews.com

**ADVANCED
ENERGY
MATERIALS**

www.advenergymat.de

analysis was performed using a JEOL USA JEM-2100F (Cs corrector) transmission electron microscope. Besides, GIWAXS were conducted at PLS-II 9A U-SAXS beamline of the Pohang Accelerator Laboratory in Korea. The X-rays coming from the in-vacuum undulator (IVU) were monochromated (wavelength λ = 1.10994 Å) using a double crystal monochromator and focused both horizontally and vertically (450 (H) × 60 (V) μm^2 in FWHM @ sample position) using K-B type mirrors. The GIWAXS sample stage was equipped with a 7-axis motorized stage for the fine alignment of sample, and the incidence angle of X-ray beam was set to be 0.11° to 0.13° for BDD-based copolymer films and blended films. GIWAXS patterns were recorded with a 2D CCD detector (Rayonix SX165) and X-ray irradiation time was 6–9 s, dependent on the saturation level of the detector. Diffraction angles were calibrated using a sucrose standard (Monoclinic, P21, a = 10.8631 Å, b = 8.7044 Å, c = 7.7624 Å, β = 102.938°) and the sample-to-detector distance was ≈231 mm. CCL was calculated according to the following Scherrer equation

$$L_c = \frac{2\pi K}{\Delta_q} \tag{2}$$

In this equation, L_c is the crystal coherence length, K is a shape factor (0.9), and Δ_q is the full width at half-maximum of a diffraction peak (FWHM).[14c,21]

Supporting Information

Supporting Information is available from the Wiley Online Library or from the author.

Conflict of Interest

The authors declare no conflict of interest.

[1] a) J.-D. Chen, C. Cui, Y.-Q. Li, L. Zhou, Q.-D. Ou, C. Li, Y. Li, J.-X. Tang, *Adv. Mater.* **2015**, *27*, 1035; b) Y. Jin, Z. Chen, S. Dong, N. Zheng, L. Ying, X.-F. Jiang, F. Liu, F. Huang, Y. Cao, *Adv. Mater.* **2016**, *28*, 9811; c) Y. Liu, J. Zhao, Z. Li, C. Mu, W. Ma, H. Hu, K. Jiang, H. Lin, H. Ade, H. Yan, *Nat. Commun.* **2014**, *5*, 5293; d) L. Lu, T. Zheng, Q. Wu, A. M. Schneider, D. Zhao, L. Yu, *Chem. Rev.* **2015**, *115*, 12666; e) K. H. Park, Y. An, S. Jung, H. Park, C. Yang,

[2] a) J. E. Anthony, A. Facchetti, M. Heeney, S. R. Marder, X. Zhan, *Adv. Mater.* **2010**, *22*, 3876; b) L. Ye, X. Jiao, M. Zhou, S. Zhang, H. Yao, W. Zhao, A. Xia, H. Ade, J. Hou, *Adv. Mater.* **2015**, *27*, 6046; c) G. Yu, J. Gao, J. C. Hummelen, F. Wudl, A. J. Heeger, *Science* **1995**, *270*, 1789.

[3] a) S. Chen, Y. An, G. K. Dutta, Y. Kim, Z.-G. Zhang, Y. Li, C. Yang, *Adv. Funct. Mater.* **2017**, *27*, 1603564; b) S. Holliday, R. S. Ashraf, C. B. Nielsen, M. Kirkus, J. A. Röhr, C.-H. Tan, E. Collado-Fregoso, A.-C. Knall, J. R. Durrant, J. Nelson, I. McCulloch, *J. Am. Chem. Soc.* **2015**, *137*, 898; c) O. K. Kwon, M. A. Uddin, J.-H. Park, S. K. Park, T. L. Nguyen, H. Y. Woo, S. Y. Park, *Adv. Mater.* **2016**, *28*, 910; d) Y. Lin, J. Wang, Z.-G. Zhang, H. Bai, Y. Li, D. Zhu, X. Zhan, *Adv. Mater.* **2015**, *27*, 1170; e) F. Liu, Z. Zhou, C. Zhang, T. Vergote, H. Fan, F. Liu, X. Zhu, *J. Am. Chem. Soc.* **2016**, *138*, 15523; f) D. Sun, D. Meng, Y. Cai, B. Fan, Y. Li, W. Jiang, L. Huo, Y. Sun, Z. Wang, *J. Am. Chem. Soc.* **2015**, *137*, 11156; g) P. M. Beaujuge, J. M. J. Fréchet, *J. Am. Chem. Soc.* **2011**, *133*, 20009; h) S. Dai, F. Zhao, Q. Zhang, T.-K. Lau, T. Li, K. Liu, Q. Ling, C. Wang, X. Lu, W. You, X. Zhan, *J. Am. Chem. Soc.* **2017**, *139*, 1336; i) J. W. Jung, J. W. Jo, C.-C. Chueh, F. Liu, W. H. Jo, T. P. Russell, A. K. Y. Jen, *Adv. Mater.* **2015**, *27*, 3310; j) L. Schmidt-Mende, A. Fechtenkötter, K. Müllen, E. Moons, R. H. Friend, J. D. MacKenzie, *Science* **2001**, *293*, 1119; k) D. Xia, D. Gehrig, X. Guo, M. Baumgarten, F. Laquai, K. Müllen, *J. Mater. Chem. A* **2015**, *3*, 11086.

[4] a) Y. Yang, Z.-G. Zhang, H. Bin, S. Chen, L. Gao, L. Xue, C. Yang, Y. Li, *J. Am. Chem. Soc.* **2016**, *138*, 15011; b) W. Zhao, D. Qian, S. Zhang, S. Li, O. Inganäs, F. Gao, J. Hou, *Adv. Mater.* **2016**, *28*, 4734.

[5] a) H. Bin, L. Gao, Z.-G. Zhang, Y. Yang, Y. Zhang, C. Zhang, S. Chen, L. Xue, C. Yang, M. Xiao, Y. Li, *Nat. Commun.* **2016**, *7*, 13651; b) H. Bin, Z.-G. Zhang, L. Gao, S. Chen, L. Zhong, L. Xue, C. Yang, Y. Li, *J. Am. Chem. Soc.* **2016**, *138*, 4657; c) L. Gao, Z.-G. Zhang, H. Bin, L. Xue, Y. Yang, C. Wang, F. Liu, T. P. Russell, Y. Li, *Adv. Mater.* **2016**, *28*, 8288; d) S. Li, L. Ye, W. Zhao, S. Zhang, S. Mukherjee, H. Ade, J. Hou, *Adv. Mater.* **2016**, *28*, 9423; e) Z. Li, K. Jiang, G. Yang, J. Y. L. Lai, T. Ma, J. Zhao, W. Ma, H. Yan, *Nat. Commun.* **2016**, *7*, 13094; f) Y. Lin, F. Zhao, Q. He, L. Huo, Y. Wu, T. C. Parker, W. Ma, Y. Sun, C. Wang, D. Zhu, A. J. Heeger, S. R. Marder, X. Zhan, *J. Am. Chem. Soc.* **2016**, *138*, 4955; g) T. Liu, Y. Guo, Y. Yi, L. Huo, X. Xue, X. Sun, H. Fu, W. Xiong, D. Meng, Z. Wang, F. Liu, T. P. Russell, Y. Sun, *Adv. Mater.* **2016**, *28*, 10008; h) H. Lu, J. Zhang, J. Chen, Q. Liu, X. Gong, S. Feng, X. Xu, W. Ma, Z. Bo, *Adv. Mater.* **2016**, *28*, 9559; i) S. M. McAfee, J. M. Topple, I. G. Hill, G. C. Welch, *J. Mater. Chem. A* **2015**, *3*, 16393; j) Z. Zheng, O. M. Awartani, B. Gautam, D. Liu, Y. Qin, W. Li, A. Bataller, K. Gundogdu, H. Ade, J. Hou, *Adv. Mater.* **2017**, *29*, 1604241.

[6] a) Y. Lin, J. Wang, Z.-G. Zhang, H. Bai, Y. Li, D. Zhu, X. Zhan, *Adv. Mater.* **2015**, *27*, 1170; b) Y. Qin, M. A. Uddin, Y. Chen, B. Jang, K. Zhao, Z. Zheng, R. Yu, T. J. Shin, H. Y. Woo, J. Hou, *Adv. Mater.* **2016**, *28*, 9416; c) B. Yang, S. Zhang, Y. Chen, Y. Cui, D. Liu, H. Yao, J. Zhang, Z. Wei, J. Hou, *Macromolecules* **2017**, *50*, 1453; d) L. Ye, X. Jiao, M. Zhou, S. Zhang, H. Yao, W. Zhao, A. Xia, H. Ade, J. Hou, *Adv. Mater.* **2015**, *27*, 6046; e) N. Bauer, Q. Zhang, J. Zhao, L. Ye, J.-H. Kim, I. Constantinou, L. Yan, F. So, H. Ade, H. Yan, W. You, *J. Mater. Chem. A* **2017**, *5*, 4886.

[7] a) J. W. Jung, F. Liu, T. P. Russell, W. H. Jo, *Energy Environ. Sci.* **2013**, *6*, 3301; b) G. Kim, S. Song, J. Lee, T. Kim, T. H. Lee, B. Walker, J. Y. Kim, C. Yang, *Adv. Energy Mater.* **2015**, *5*, 1500844; c) G.-W. Kim, G. Kang, J. Kim, G.-Y. Lee, H. I. Kim, L. Pyeon, J. Lee, T. Park, *Energy*

Energy Environ. Sci. **2016**, *9*, 3464; f) V. Vohra, K. Kawashima, T. Kakara, T. Koganezawa, I. Osaka, K. Takimiya, H. Murata, *Nat. Photonics* **2015**, *9*, 403; g) S. Zhang, L. Ye, J. Hou, *Adv. Energy Mater.* **2016**, *6*, 1502529; h) J. Huang, C.-Z. Li, C.-C. Chueh, S.-Q. Liu, J.-S. Yu, A. K. Y. Jen, *Adv. Energy Mater.* **2015**, *5*, 1500406.

**ADVANCED
SCIENCE NEWS**
www.advancedsciencenews.com

**ADVANCED
ENERGY
MATERIALS**
www.advenergymat.de

Environ. Sci. **2016**, *9*, 2326; d) Z. Li, X. Xu, W. Zhang, X. Meng, W. Ma, A. Yartsev, O. Inganäs, M. R. Andersson, R. A. J. Janssen, E. Wang, *J. Am. Chem. Soc.* **2016**, *138*, 10935; e) S. Sharma, N. B. Kolhe, V. Gupta, V. Bharti, A. Sharma, R. Datt, S. Chand, S. K. Asha, *Macromolecules* **2016**, *49*, 8113.

[8] a) W. Li, K. H. Hendriks, W. S. C. Roelofs, Y. Kim, M. M. Wienk, R. A. J. Janssen, *Adv. Mater.* **2013**, *25*, 3182; b) I. McCulloch, M. Heeney, C. Bailey, K. Genevicius, I. MacDonald, M. Shkunov, D. Sparrowe, S. Tierney, R. Wagner, W. Zhang, M. L. Chabinyc, R. J. Kline, M. D. McGehee, M. F. Toney, *Nat. Mater.* **2006**, *5*, 328.

[9] D. Qian, L. Ye, M. Zhang, Y. Liang, L. Li, Y. Huang, X. Guo, S. Zhang, Z. a. Tan, J. Hou, *Macromolecules* **2012**, *45*, 9611.

[10] T. Liu, X. Pan, X. Meng, Y. Liu, D. Wei, W. Ma, L. Huo, X. Sun, T. H. Lee, M. Huang, H. Choi, J. Y. Kim, W. C. H. Choy, Y. Sun, *Adv. Mater.* **2017**, *29*, 1604251.

[11] a) D. Dang, W. Chen, R. Yang, W. Zhu, W. Mammo, E. Wang, *Chem. Commun.* **2013**, *49*, 9335; b) T. E. Kang, K.-H. Kim, B. J. Kim, *J. Mater. Chem. A* **2014**, *2*, 15252; c) J. W. Lee, H. Ahn, W. H. Jo, *Macromolecules* **2015**, *48*, 7836.

[12] Z.-G. Zhang, B. Qi, Z. Jin, D. Chi, Z. Qi, Y. Li, J. Wang, *Energy Environ. Sci.* **2014**, *7*, 1966.

[13] K.-G. Lim, J.-M. Park, H. Mangold, F. Laquai, T.-L. Choi, T.-W. Lee, *ChemSusChem* **2015**, *8*, 337.

[14] a) W. Chen, T. Xu, F. He, W. Wang, C. Wang, J. Strzalka, Y. Liu, J. Wen, D. J. Miller, J. Chen, K. Hong, L. Yu, S. B. Darling, *Nano Lett.* **2011**, *11*, 3707; b) H. Hu, K. Jiang, G. Yang, J. Liu, Z. Li, H. Lin, Y. Liu, J. Zhao, J. Zhang, F. Huang, Y. Qu, W. Ma, H. Yan, *J. Am. Chem. Soc.* **2015**, *137*, 14149; c) J. Rivnay, S. C. B. Mannsfeld, C. E. Miller, A. Salleo, M. F. Toney, *Chem. Rev.* **2012**, *112*, 5488;

d) L. Ye, W. Zhao, S. Li, S. Mukherjee, J. H. Carpenter, O. Awartani, X. Jiao, J. Hou, H. Ade, *Adv. Energy Mater.* **2017**, *7*, 1602000.

[15] a) A. L. Ayzner, C. J. Tassone, S. H. Tolbert, B. J. Schwartz, *J. Phys. Chem. C* **2009**, *113*, 20050; b) M. Campoy-Quiles, T. Ferenczi, T. Agostinelli, P. G. Etchegoin, Y. Kim, T. D. Anthopoulos, P. N. Stavrinou, D. D. C. Bradley, J. Nelson, *Nat. Mater.* **2008**, *7*, 158; c) B. J. Moon, G.-Y. Lee, M. J. Im, S. Song, T. Park, *Nanoscale* **2014**, *6*, 2440.

[16] a) M. Li, Y. Liu, W. Ni, F. Liu, H. Feng, Y. Zhang, T. Liu, H. Zhang, X. Wan, B. Kan, Q. Zhang, T. P. Russell, Y. Chen, *J. Mater. Chem. A* **2016**, *4*, 10409; b) J. Yuan, L. Qiu, Z.-G. Zhang, Y. Li, Y. Chen, Y. Zou, *Nano Energy* **2016**, *30*, 312; c) K. Zhao, Q. Wang, B. Xu, W. Zhao, X. Liu, B. Yang, M. Sun, J. Hou, *J. Mater. Chem. A* **2016**, *4*, 9511; d) W. Zhao, D. Qian, S. Zhang, S. Li, O. Inganäs, F. Gao, J. Hou, *Adv. Mater.* **2016**, *28*, 4734.

[17] a) S. R. Cowan, A. Roy, A. J. Heeger, *Phys. Rev. B* **2010**, *82*, 245207; b) A. K. K. Kyaw, D. H. Wang, V. Gupta, W. L. Leong, L. Ke, G. C. Bazan, A. J. Heeger, *ACS Nano* **2013**, *7*, 4569; c) I. Riedel, J. Parisi, V. Dyakonov, L. Lutsen, D. Vanderzande, J. C. Hummelen, *Adv. Funct. Mater.* **2004**, *14*, 38; d) P. Schilinsky, C. Waldauf, C. J. Brabec, *Appl. Phys. Lett.* **2002**, *81*, 3885.

[18] H. Kim, J. Byun, S.-H. Bae, T. Ahmed, J.-X. Zhu, S.-J. Kwon, Y. Lee, S.-Y. Min, C. Wolf, H.-K. Seo, J.-H. Ahn, T.-W. Lee, *Adv. Energy Mater.* **2016**, *6*, 1600172.

[19] L. J. A. Koster, V. D. Mihailetchi, R. Ramaker, P. W. M. Blom, *Appl. Phys. Lett.* **2005**, *86*, 123509.

[20] H. Bin, Y. Yang, Z.-G. Zhang, L. Ye, M. Ghasemi, S. Chen, Y. Zhang, C. Zhang, C. Sun, L. Xue, C. Yang, H. Ade, Y. Li, *J. Am. Chem. Soc.* **2017**, *139*, 5085.

[21] S. Li, W. Liu, C.-Z. Li, F. Liu, Y. Zhang, M. Shi, H. Chen, T. P. Russell, *J. Mater. Chem. A* **2016**, *4*, 10659.